Visualization of Therapeutic Ultrasonic Beams using Fringe Patterns-based Background-Oriented Schlieren Imaging and Hilbert Transformation

Margi Sasono[1]

[1] *Study Program of Physics, Ahmad Dahlan University, Yogyakarta, Indonesia*

Abstract

Use of ultrasonic wave in medicals requires a safe treatment for human bodies (patients). The uncontrolled intensities of the ultrasonic sources cause ineffective treatment to the patient. The intensity as a main physical parameter have to be set and controlled accurately. So far, the hydrophone probe method provides a gold standard in providing the ultrasonic intensity visualization. However, this method has constraints such as time-consuming, intrusive, and off-axis measurements. In this letter, an optical method called background-oriented schlieren (BOS) imaging has been developed as an alternative to the hydrophone probe method. This optical method uses a background of fringe (line) patterns (similar to sinusoidal pattern) captured by a digital camera. The ultrasonic wave in the water displaces the fringe patterns relative to the background reference. A Hilbert Transform (HT) has been used to estimate the displacement of sinusoidal patterns proportional to the phase difference with a sinusoidal reference background, and reconstruct it as an ultrasonic intensity visualization. This letter reports that the developed BOS imaging capable of visualizing the ultrasound intensity (field) produced by a 1-MHz frequency therapeutic transducer operated in continuous-wave (CW) mode. The visualization results show a sinusoidal mode of the phase difference and the amplitude mode proportional to the ultrasound intensities. Thus, the developed BOS imaging is promising to be used as a calibration device of ultrasound beams or accuracy assessment to ensure patient safety in medicals.

Keywords: *Visualization, Ultrasonic, Fringe, Schlieren, Imaging, Hilbert*

1. Introduction

Visualization of ultrasonic beams is essential in ensuring safety aspects in medical applications such as diagnosis [1], therapeutic [2], and surgery [3]. In the metrology field, hydrophone scanning has provided a gold method to visualize the ultrasonic beams of a medical transducer according to the standard of ISO/IEC 61689:2022 [4]. However, several issues, including intrusive methods, off-axis measurement, and time-consuming, hamper its widespread use in metrology [5].

As an alternative, the optical method-based schlieren imaging has found commercial use in the visualization of ultrasonic beams [6]. However, this device also has several drawbacks, such as the need for precise optical component alignment, a limited field of view (FOV), and low sensitivity to the acousto-optics effect [5]. Schlieren imaging is still not a standard in ultrasonic beam metrology

On the other, background-oriented schlieren imaging (BOSI) is a variant of schlieren imaging. Unlike schlieren imaging, the BOSI setup needs background patterns and a digital camera. The visualization technique relies on the change in density (schlieren object). A camera captures this change as a distorted background pattern to visualize the physical characteristics of a schlieren object. Hence, the BOSI has recently found a wide range of applications, including the qualitative visualization of fluid flow [7], aerodynamics [8], shock waves [9], and many others. In its development, the BOSI has enabled quantitative measurement of refractive index [10] and medium density [11].

Ultrasonic beams can be visible with BOSI [12] . In principle, the propagation of ultrasonic waves in water causes a change in refractive index due to changes in water density. If the light rays propagating from the background pattern pass through the refractive index variations, an acousto-optics effect will occur [13]. A BOSI camera records this effect as a distorted pattern image that contains information about the ultrasonic beams. Thus, the type of background pattern is critical to improve BOSI visualizations.

Generally, a BOSI setup uses random dot patterns and digital image correlation (DIC) as the image processing algorithm [14]. However, the distribution of dots on the background plane can be uneven, and the large density changes in the medium can distort the shape of the dots [15]. Therefore, in recent years, BOSI has considered periodic patterns as the background [16].

This letter proposes the new development of the BOSI technique using a fringe pattern (instead of random dots) as a background with Hilbert Transform (HT) phase demodulation as an image processing method. The work in this letter tests the developed BOSI to visualize the ultrasonic beams emitting from a therapeutic transducer. This work relies on the principle that the refractive index variations due to ultrasonic beams in water introduce the light deflection proportional to the phase-modulated light rays. The BOSI camera detects this deflection and captures it as a displacement of fringe patterns. Hence, this letter proposes the HT phase demodulation to extract the phase of modulated light rays based on the fringe displacements related to the refractive index variations for visualizing the ultrasonic beams. Previous studies have demonstrated that the fringe patterns outperform the random dot as background for improving the BOSI measurement [16]. Also, the phase demodulation technique has proven to be accurate for designing a phase microscopy device [17]. This letter expects that the developed BOSI can visualize the accurate shape of the ultrasonic beams and improve the field of metrology in calibrating an ultrasonic transducer.

2. Experiments

The BOSI principle is straightforward optically, as seen in Fig. 1. The distance between the background patterns and the camera is $Z \gg f$, where f is the lens's focal length. This arrangement enables the parallel light rays along the z-axis (optical axis) by assuming the background position from the camera is infinite [18]. The position of a schlieren object (refractive index variations) is Z_{T} from the background, between the background and the camera. A light ray from the background patterns travels to the camera through the schlieren object. A mathematical model can describe a light ray path in the schlieren object along the z-axis as [19]

$$\frac{d^2y}{dz^2} = \frac{1}{n}\left(\frac{dn}{dy}\right) \tag{1}$$

where n is the refractive index, and (dn/dy) represents refractive index variations (or refractive index gradient) of a schlieren object under test. Equation (1) states the curvature of a deflected ray in proportion to the strength of the refractive index gradient. As shown in Fig. 1, a reference light ray (dashed line) has no deflection toward the camera. The changes in the refractive index lead to a light ray deflection, as depicted by the solid lines in Fig. 1. The camera captures this deflection as a displacement in the position of the light ray incident on the camera (image plane).

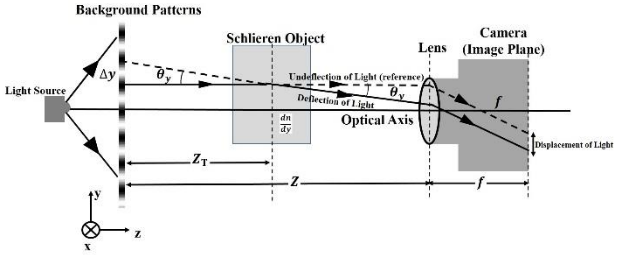

Fig. 2 The principle of BOSI.

Integrating Eq. (1) gives a relationship between the deflection angle and the displacement fringe pattern as

$$\theta_y \approx \left(\frac{dy}{dz}\right) = \left(\frac{\Delta y}{Z_{\mathrm{T}}}\right) = \frac{1}{n}\int\left(\frac{dn}{dy}\right)dz \tag{2}$$

where θ_y is the deflection angle along the y-axis, Δy is a displacement of fringe patterns in the background plane (virtual displacement) due to the displacement of the light ray incident on the camera (image plane), and Z_{T} denotes a distance between the schlieren object and the background. The magnitude of the deflection angle in Eq.(2) depends on the fringe displacements in the background plane and the refractive index gradient. The BOSI is thus sensitive to measuring the light ray deflection angles.

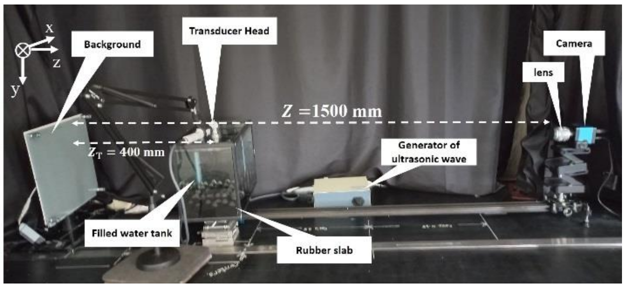

Fig. 2 Setup implementation of developed BOSI.

The photograph in Fig. 2 shows how a BOSI implementation only needs a background pattern and a camera as the two main components. This simplicity can reduce the measurement error caused by the optical component misalignment [20]. A developed background was a horizontal fringe pattern in black-and-white variations printed on 30 cm × 30 cm transparent media. The thickness of each fringe was 1 mm. As a light source for the background illumination was a white LED Panel commercial. This work records the BOSI images using a Hayear model digital camera with an image resolution of 1080 pixels × 1920 pixels and a spatial resolution of 1.43 μm. A lens mounted on the camera was a Fujian model with a focal length of $f = 50$ mm. While capturing images, the lens focuses on the patterns in the background. The distance between the background and the camera lens is $Z = 1500$ mm, and distance from the background to the transducer head is $Z_\mathrm{T} = 400$ mm.

A 40 cm × 40 cm filled water tank with a transparent wall provides the medium for propagating an ultrasonic wave emitted by a transducer under test. The position of the tank was between the background and the camera. The technique for propagating the ultrasonic waves is to immerse the transducer head a few millimetres into the water with its face parallel to the bottom of the tank. Also, the design attaches a 50 mm thick rubber slab at the bottom of the tank to prevent the ultrasonic waves from back-reflecting to the transducer. This work tests the developed BOSI to visualize the ultrasonic beam of a therapeutic transducer operating in continuous-wave (CW) mode at a frequency of 1 MHz and an intensity of 1 W/cm^2.

The propagation of ultrasonic waves in water causes the pressure wave and generates refractive index variations due to the changes in water density. The variations are similar to phase grating (grids) in the optical diffractions principle [13]. When passing through the refractive index variations, the light rays from the background pattern diffract (deflect) at a specific angle. The light rays also undergo the phase modulation caused by the differences in optical path lengths across the refractive index variations [21]. The BOSI camera captures this modulation as an image of fringe displacement relative to the reference fringe (without the ultrasonic beam).

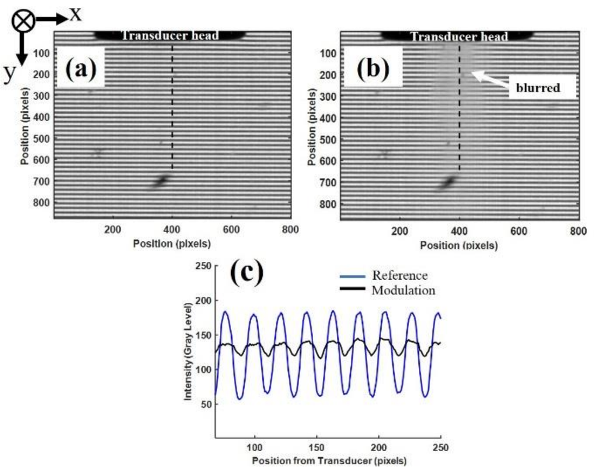

Fig. 3 Raw images as captured by camera. (a) Reference. (b) Modulation. (c) Comparison of image intensity distribution in column 400 as indicated by black dashed lines in (a) and (b).

The photographs captured by a camera, as shown in Fig.3, compare the raw images of reference (without the ultrasonic beams) and modulation (with the ultrasonic beams). Once the transducer emits the ultrasonic beams, a modulation image appears blurred at a given region, as shown in Fig. 3b. As observed, the fringe patterns were distorted when compared to the raw image of reference in Fig.3a. It is strongly suspected that a blurred and distorted image indicates the presence of ultrasonic beams emitting from a transducer head.

As shown in Fig.3c, the image intensity distribution in column 400 (only 150 gray-level data of black dashed lines in Figs. 3a and 3b) reveals a comparison between the reference (blue solid curve) and modulated (modulation) intensity (black dashed curve). As seen, there is a significant difference in both curves. The intensity magnitude on the modulated curve decreases compared to the reference curve. This decrease shows that the light rays emanating from the background pattern undergo the absorption due to the ultrasonic beams. Also, the phase-difference between the two curves is insignificant. Without any image processing method, the developed BOSI can already detect the presence of ultrasonic beams. However, this result is a qualitative visual, whereas the metrology field requires both qualitative and quantitative results.

A mathematical model can represent the reference sinusoidal curve in the y-axis as [22]

$$I_\mathrm{R}(y) = I_\mathrm{OR} \cos \varphi_\mathrm{R}(y) \tag{3}$$

where $I_\mathrm{R}(y)$ is the reference intensity distribution along the y-axis, I_OR is the magnitude of reference intensity, and $\varphi_\mathrm{R}(y)$ denotes the reference phase along the y-axis. Similarly, a mathematical model of a modulated sinusoidal curve is

$$I_\mathrm{M}(y) = I_\mathrm{OM} \cos \varphi_\mathrm{M}(y) \tag{4}$$

where, $I_\mathrm{M}(y)$ is the modulated intensity distribution along the y-axis, I_OM is the magnitude of modulated intensity, and $\varphi_\mathrm{M}(y)$ represents a phase modulation related to the physical quantity to be measured. Subtracting Eq. (4) from Eq. (3) leads to the phase-difference as

$$\Delta\varphi\ (y) = \varphi_\mathrm{R}(y) - \varphi_\mathrm{M}(y) \tag{5}$$

where, $\Delta\varphi\ (y)$ is the phase difference between reference and modulation curves (in rad). As stated in Eq.(5), the phase difference is essential to quantify the physical information of ultrasonic beams emitted by a transducer under test.

This work assumes that the intensity in Eqs. (3) and (4) are real-valued data of experiment results [22]. In terms of signal theory, applying the HT to Eqs. (3) and (4) yield an analytical signal in the complex-valued data as

$$Z(y) = Z_\mathrm{RE}(y) + i\, Z_\mathrm{IM}(y) = A(y)e^{i\phi(y)} \tag{6}$$

where, $Z(y)$ is an analytical signal, $Z_\mathrm{RE}(y)$ is the real-valued data (signal), $i = \sqrt{-1}$ is the imaginary number, $Z_\mathrm{IM}(y)$ is imaginary-valued data, $A(y)$ is magnitude of intensity (envelope of signal or amplitude), and $\phi(y)$ denotes a phase of analytical signal. Mathematically, it is convenient to obtain a phase signal in Eq. (6) as [22]

$$\phi(y)=\arctan\left[\frac{Z_{\mathrm{IM}}(y)}{Z_{\mathrm{RE}}(y)}\right] \text{ in radian} \qquad (7)$$

The phase signal calculated by Eq. (7) is wrapped in range $(-\pi,\ +\pi)$ due to the mathematical characteristics of an arctan function. Therefore, this work needs an unwrapping process to obtain the desired phase. The details of this unwrapping process are beyond the scope of this letter. In addition, using Eq.(6) also gives information on the magnitude of the intensity or amplitude of a signal.

The HT method transforms column-by-column the pixels in the raw images in Figs.3a and 3b. The process is similar to the scanning raster across the image plane. As shown in Fig. 4, a series of images shows the application of the HT method for extracting the phase in the BOSI images. All computations in this work use a MATLAB environment. A MATLAB Hilbert function transforms the image intensity distribution in Figs.3a and 3b into the complex-valued data (signal). Next, the MATLAB arctan function calculates the wrapped phase of the reference and modulation images, as shown in Figs.4a and 4b, respectively. The phase distributions in column 400 (a segment of white dashed lines in Figs.4a and 4b) show the wrapped phase curves in range $(-\pi,\ +\pi)$ of reference (Fig.4c) and modulation (Fig.4d) according to Eq.(7).

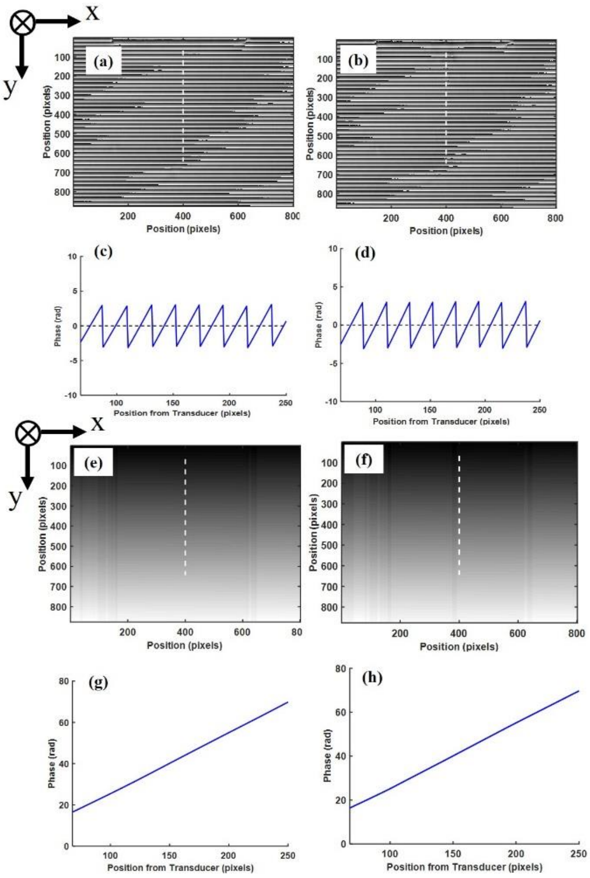

Fig. 4 Extracting phase of raw images using the HT method. (a) Wrapped phase of reference image. (b) Wrapped phase of modulation image. Wrapped phase curves of reference (c) and modulation (d) in column 400 as indicated by white dashed lines in (a) and (b). (e) Unwrapped phase of reference image. (f) Unwrapped phase of modulation image. Unwrapped phase curves of reference (g) and modulation (h) in column 400 as indicated by white dashed lines in (e) and (f).

The unwrapping process using MATLAB unwrap function of Figs. 4a and 4b lead to the unwrapped phase images, as shown in Fig. 4e (reference) and Fig. 4f (modulation). The phase distributions in column 400 (a segment of white dashed lines in Figs. 4e and 4f) show the unwrapped phase curves of reference (Fig.4g) and modulation (Fig.4h). As observed, the unwrapped phase curves have spatially linear characteristics, as outlined in [23].

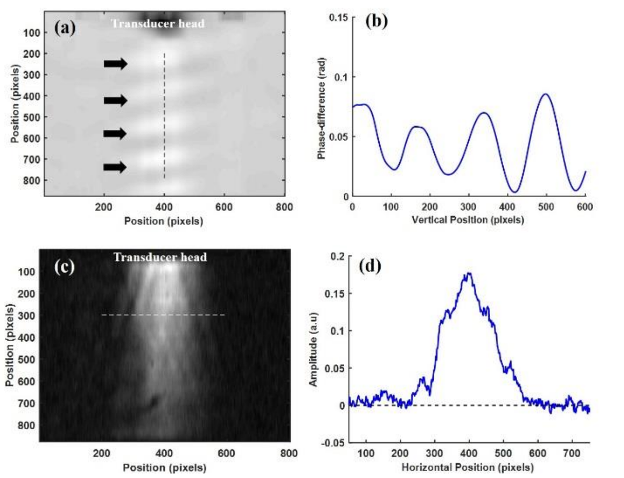

Fig. 5 (a) Reconstructed phase-difference image. (b) Plot of phase-difference data along black dashed lines (vertical position in column 400). (c) Reconstructed amplitude image. (d) Plot of amplitude data along white dashed lines (horizontal position in row 300).

As shown in Fig.5a, subtracting the unwrapped phase in Fig.4f from Fig.4e yields a phase-difference image related to the 2-D physical characteristics of the density changes in water due to the propagation of ultrasonic beams. As observed, the image reveals the bright-dark variations (brightness variations as indicated by the arrows). This phase-difference variation is suspected to represent a change in water density, which in turn describes the ultrasonic pressure wave.

As shown in Fig.5b, the phase-difference data of column 400 along the black dashed lines in Fig.5a reveals an undulation curve similar to the physical characteristics of a harmonic wave. This undulation may be related to the compression and rarefaction of water density under the influence of ultrasonic pressure waves, as the principle of a sound wave outlined in [24]. On the other side, Fig.5c shows an amplitude image obtained by the HT method. Visually, there is a significant difference between the phase-difference image (Fig.5a) and the amplitude image (Fig.5c). The phase-difference image describes the variations of the phase of light related to the changes in water density. On the other hand, the amplitude image represents the light intensity variations as captured by a conventional camera. As shown in Fig.5d, the amplitude data of row 300 along the white dashed lines in Fig.5c reveals a curve describing the amplitude distribution proportional to the distribution of ultrasonic beam intensity parallel to the face of a transducer head. As shown in Fig.5d, the curve is similar to a Gaussian shape that exhibits high intensity at the centre of the transducer head under test. The curve width can be related to the ultrasonic beam width, as outlined in [25]. Therefore, both curves (Figs. 5b and 5d) can be the basis for obtaining detailed physical information about the ultrasonic waves emitted from a transducer head under test.

3. Conclusions

This letter has successfully developed the BOSI technique using the proposed fringe patterns (instead of the random dots) background and the HT method for visualizing the ultrasonic beams emitted by a therapeutic transducer. The developed BOSI successfully converts the fringe displacements in the background into the phase-difference and amplitude data. The BOSI then reconstructs the data into images representing an ultrasonic beam. The result also shows that the phase-difference and amplitude images differ significantly. However, both images can be essential for obtaining detailed physical information about the ultrasonic beams. The developed BOSI offers the advantages such as simple, rapid, 2-D visualization and non-intrusive techniques. Hence, the developed BOSI can potentially improve the calibrating of ultrasonic waves emitting from a transducer.

References

[1] I. Akiyama, “Basic and recent applied technologies of ultrasound in the field of clinical diagnosis,” *Acoust. Sci. Technol.*, vol. 41, no. 6, pp. 845–850, 2020.

[2] D. Draper and R. M Mallipudi, “Therapeutic ultrasound: myths and truths for nonportable in-clinic and portable home use ultrasound,” *MOJ Sport. Med.*, vol. 4, no. 4, pp. 115–116, 2020.

[3] M. Hofmann, A. Haeberlin, S. de Brot, A. Stahel, H. Keppner, and J. Burger, “Development and evaluation of a titanium-based planar ultrasonic scalpel for precision surgery,” *Ultrasonics*, vol. 130, no. May 2022, p. 106927, 2023.

[4] G. R. Harris *et al.*, “Hydrophone Measurements for Biomedical Ultrasound Applications: A Review,” *IEEE Trans. Ultrason. Ferroelectr. Freq. Control*, vol. 70, no. 2, pp. 85–100, 2023.

[5] G. Xing, V. Wilkens, and P. Yang, “Review of field characterization techniques for high intensity therapeutic ultrasound,” *Metrologia*, vol. 58, no. 2, 2021.

[6] M. D. Dunlap, J. Beach, and T. Massey, “Ultrasound beam characterization through real time visualization with schlieren imaging,” *IEEE Int. Ultrason. Symp. IUS*, vol. 2020-September, pp. 0–3, 2020.

[7] M. Yamagishi *et al.*, “Quantitative density measurement of wake region behind reentry capsule (Improvements in accuracy of 3D reconstruction by

evaluating the view-angle of measurement system)," *J. Fluid Sci. Technol.*, vol. 16, no. 3, pp. 1–10, 2021.

[8] H. Ding, S. Yi, and X. Zhao, "Experimental investigation of aero-optics induced by supersonic film based on near-field background-oriented schlieren," *Appl. Opt.*, vol. 58, no. 11, p. 2948, 2019.

[9] T. Mizukaki, T. Odagiri, T. Matsumura, and K. Wakabayashi, "Quantitative flow visualization of a blast wave from an underground magazine model using backgroundoriented schlieren," *Sci. Tech. Energ. Mater.*, vol. 81, no. 5, pp. 128–136, 2020.

[10] S. J. Grauer and A. M. Steinberg, "Fast and robust volumetric refractive index measurement by unified background-oriented schlieren tomography," *Exp. Fluids*, vol. 61, no. 3, 2020.

[11] Y. Kaneko, H. Nishida, and Y. Tagawa, "Background-oriented schlieren measurement of near-surface density field in surface dielectric-barrier-discharge," *Meas. Sci. Technol.*, vol. 32, no. 12, 2021.

[12] M. Colom, P. Ricci, and M. Duocastella, "Rapid quantification of 3D ultrasound fields with wavefront sensing and Schlieren tomography," *Ultrasonics*, vol. 135, no. April, p. 107115, 2023.

[13] B. Shen *et al.*, "Accuracy optimization method of ultrasonic power measurement system based on acousto-optic effect," *Opt. Rev.*, vol. 28, no. 2, pp. 207–214, 2021.

[14] T. Shimazaki, S. Ichihara, and Y. Tagawa, "Background oriented schlieren technique with fast Fourier demodulation for measuring large density-gradient fields of fluids," *Exp. Therm. Fluid Sci.*, vol. 134, no. January, p. 110598, 2022.

[15] M. Meinecke, A. Kilzer, and E. Weidner, "Background Orientated Schlieren Method Applied for Liquid Systems of Strong Refractive Gradients," *Chemie-Ingenieur-Technik*, vol. 92, no. 8, pp. 1089–1097, 2020.

[16] N. A. Vinnichenko, A. V. Pushtaev, Y. Y. Plaksina, and A. V. Uvarov, "Performance of Background Oriented Schlieren with different background patterns and image processing techniques," *Exp. Therm. Fluid Sci.*, vol. 147, no. April, p. 110934, 2023.

[17] F. Nienhaus, T. Piotrowski, B. Nießing, N. König, and R. H. Schmitt, "Adaptive phase contrast microscopy to compensate for the meniscus effect," *Sci. Rep.*, vol. 13, no. 1, pp. 1–11, 2023.

[18] C. Schwarz and J. N. Braukmann, "Practical aspects of designing background-oriented schlieren (BOS) experiments for vortex measurements," *Exp. Fluids*, vol. 64, no. 4, pp. 1–19, 2023.

[19] L. Wei, H. Qi, G. Li, S. T. Ruan, and H. Li, "Tomographic reconstruction of refractive index fields based on laser beam deflection measurement," *Opt. Commun.*, vol. 492, no. March, p. 126951, 2021.

[20] M. Raffel, "Background-oriented schlieren (BOS) techniques," *Exp. Fluids*, vol. 56, no. 3, pp. 1–17, 2015.

[21] H. Kun Zheng *et al.*, "A novel high accuracy optical path difference compensation method based on phase difference technology," *Opt. Lasers Eng.*, vol. 137, no. July 2020, p. 106367, 2021.

[22] J. Zhu, Y. Wu, H. Yue, and X. Shao, "Single frame phase estimation based on Hilbert transform and Lissajous Ellipse Fitting method in fringe projection technology," *Opt. Commun.*, vol. 488, no. January, p. 126817, 2021.

[23] X. Meng, F. Wang, J. Liu, M. Chen, and Y. Wang, "Phase shifting profilometry based on Hilbert transform: An efficient phase unwrapping algorithm," *J. Appl. Phys.*, vol. 131, no. 19, 2022.

[24] A. M. Goldfain, C. S. Yung, K. A. Briggman, and J. Hwang, "Optical phase contrast imaging for absolute, quantitative measurements of ultrasonic fields with frequencies up to 20 MHz," *J. Acoust. Soc. Am.*, vol. 149, no. 6, pp. 4620–4629, 2021.

[25] K. Zeng *et al.*, "Induction of Human Motor Cortex Plasticity by Theta Burst Transcranial Ultrasound Stimulation," *Ann. Neurol.*, vol. 91, no. 2, pp. 238–252, 2022.

* asj-editcom-sec@acoustics.jp